

Formaldehyde and methanol formation from reaction of carbon monoxide and hydrogen on neutral Fe₂S₂ clusters in the gas phase

Cite this: *Phys. Chem. Chem. Phys.*, 2013, **15**, 4699

Shi Yin, Zhechen Wang and Elliot R. Bernstein*

Reaction of CO with H₂ on neutral Fe_mS_n clusters in a fast flow reactor is investigated both experimentally and theoretically. Single photon ionization at 118 nm is used to detect neutral cluster distributions through time of flight mass spectrometry. Fe_mS_n clusters are generated through laser ablation of a mixed iron–sulfur target in the presence of a pure helium carrier gas. A strong size dependent reactivity of (FeS)_m clusters toward CO is characterized. The reaction FeS + CO → Fe + OCS is found for the FeS cluster, and the association product Fe₂S₂CO is observed for the Fe₂S₂ cluster. Products Fe₂S₂¹³COH₂ and Fe₂S₂¹³COH₄ are identified for reactions of ¹³CO and H₂ on Fe₂S₂ clusters: this suggests that the Fe₂S₂ cluster has a high catalytic activity for hydrogenation reactions of CO to form formaldehyde and methanol. Density functional theory (DFT) calculations are performed to explore the potential energy surfaces for the two reactions: Fe₂S₂ + CO + 2H₂ → Fe₂S₂ + CH₃OH; and Fe₂S₂ + CO + H₂ → Fe₂S₂ + CH₂O. A barrierless, thermodynamically favorable pathway is obtained for both catalytic processes. Catalytic cycles for formaldehyde and methanol formation from CO and H₂ on a Fe₂S₂ cluster are proposed based on our experimental and theoretical investigations. The various reaction mechanisms explored by DFT are in good agreement with the experimental results. Condensed phase iron sulfide, which contains exposed Fe₂S₂ units on its surface, is suggested to be a good catalyst for low temperature formaldehyde/methanol synthesis.

Received 15th January 2013,
Accepted 6th February 2013

DOI: 10.1039/c3cp50183c

www.rsc.org/pccp

Introduction

Methanol synthesis from carbon monoxide and hydrogen, (CO + 2H₂ → CH₃OH, ΔH° = −94.47 kJ mol^{−1}, ΔG° = −29.17 kJ mol^{−1}) is an important industrial process, and it offers a clear economic and political advantage compared with oil refining.¹ Methanol is not only an essentially fundamental feedstock for the chemical industry but it is also a clean liquid fuel and can be utilized in automobiles and other (e.g., fuel cell) applications.^{2–4} The syngas (CO + H₂) catalytic reaction to produce CH₃OH has attracted deep interest for nearly a century.^{5,6} A “methanol economy” has also raised interest in sustainable energy studies.^{7,8} Commercially, methanol can be synthesized from carbon monoxide and hydrogen over a Cu/ZnO catalyst under severe conditions, 250–300 °C and 50–100 atmospheres.^{5,6} Efficiency of the industrial methanol process is severely limited by thermodynamics. For example, at 300 °C and 50 atm, the theoretical maximum CO

conversion is around 20%.⁹ As a means to reduce the production costs and to utilize the thermodynamic merit of this reaction, low-temperature synthesis of methanol is challenging and important.¹⁰ Many catalysis studies are done on condensed phase reactions.^{11–17} For example, high catalytic activity for the reaction CO + 2H₂ → CH₃OH can be produced with ceria supported copper catalysts prepared by a coprecipitation method at a reaction temperature below 200 °C.^{11,12} In comparison with commercial copper–zinc catalysts, the equivalent activity is obtained at a lower reaction temperature by 60 °C. Almost 40% of the produced methanol is converted to formaldehyde over iron molybdenum oxide catalysts.^{18–20} The selective oxidation of methanol to formaldehyde is widely studied on Fe₂O₃, MoO₃, and an industrial iron molybdate catalyst.^{18,21–24} As formaldehyde is manufactured on an industrial scale by methanol oxidation, it is another particularly desirable product of the carbon monoxide hydrogenation process.

Since clusters are good model systems for active site simulation of complex solid state catalysts, and atomic/molecular level mechanisms for condensed phase catalytic reactions may be understood through the study of model reactions,^{25–32} a number

Department of Chemistry, NSF ERC for Extreme Ultraviolet Science and Technology, Colorado State University, Fort Collins, CO 80523, USA.
E-mail: erb@lamar.colostate.edu

of studies have been carried out for the reaction of metal–metal oxide–metal sulfide clusters with CO and H₂. Adsorption dynamics of CO on silica supported nanofabricate CuO_x clusters have been investigated by utilizing electron beam lithography to study methanol synthesis model systems.³³ CO binding energies on oxidic clusters are found to be larger than for metallic clusters, but metallic Cu clusters are more reactive than oxidic clusters, in part not only due to cluster size effects, but apparently also because of electronic effects. Reactions of carbon monoxide and/or hydrogen with various metal and metal compound (e.g., Ni_n,³⁴ V_n,^{35,36} Nb_n^{+0/-},³⁵⁻³⁹ and Mo_xS_y^{40,41}) clusters have been reported. The reactivity of CO and H₂ (D₂) with these clusters exhibits strong size dependence. Neutral Nb₈, Nb₁₀, and Nb₁₆ clusters are far less generally reactive with CO and H₂ than are their neighbor Nb_n clusters.^{35,37} The reactivity of neutral Nb_n with CO smoothly increases for $n \geq 3$ with no adsorbed products detected for $n = 1$ and 2.³⁶ Methanol can be formed exclusively on Nb₈ in the reaction of neutral Nb_n clusters with CO + H₂.³⁹ The neutral Mo₆S₈ cluster is predicted to have moderate activity for converting CO and H₂ to methanol.⁴⁰

Recently, interest in iron sulfur clusters arises from their role as active centers of proteins,^{42,43} and their great significance in both industrial and biochemical catalysis.⁴⁴⁻⁴⁷ A number of studies have been performed on gas phase iron sulfur clusters for investigation of their composition, stability, and structure;⁴⁸⁻⁵⁹ nevertheless, little is known about reactive and catalytic properties of small neutral iron sulfur clusters. In this paper, reactions of neutral iron sulfur clusters with CO and H₂ are studied by 118 nm single photon ionization (SPI) coupled with time-of-flight mass spectrometry (TOFMS): ¹³CO is employed to identify hydrogenation reaction products. Detailed reaction mechanisms are suggested for the formation of CH₂O and CH₃OH based on the experimental observations and theoretical calculations.

Methods

A. Experimental procedures

The experimental setup for laser ablation coupled with a fast flow reactor employed in this work has been described previously in detail.⁶⁰⁻⁶⁴ Only a brief outline of the apparatus is given below. Fe_mS_n clusters are generated by laser ablation of a mixed iron–sulfur target in the presence of a pure helium carrier gas (99.99%, General Air). The target is made by pressing a mixture of iron (99.9%, Sigma Aldrich) and sulfur (99.98%, Sigma Aldrich) powders. A 10 Hz, focused, 532 nm Nd³⁺:YAG laser (Nd³⁺:yttrium aluminum garnet) with ~6 mJ per pulse energy is used for the laser ablation. The expansion gas is pulsed into the vacuum by a supersonic nozzle (R. M. Jordan, Co.) with a backing pressure of typically 75 psi. Generated iron sulfide clusters react with reactants in a fast flow reactor (i.d. 6.3 mm × 76 mm), which is directly coupled to the cluster generation channel (i.d. 1.8 mm × 19 mm). The reactant gases, CO or ¹³CO (99.5% Sigma Aldrich) seeded in a pure helium or hydrogen gas, with a 20 psi backing pressure, are injected into the reactor by a pulsed General Valve (Parker, Serial 9). Timing between the Jordan valve and the General Valve opening is optimized for the

best product yields. The pressure in the fast flow reactor can be estimated as 14 Torr for the reaction and the collision rate between vanadium sulfide clusters and helium is estimated *ca.* 10⁸ s⁻¹.⁶⁵ Reactants and products are thermalized to 300–400 K by collision after the reaction.⁶⁶ An electric field is placed downstream of the reactor in order to remove any residual ions from the molecular beam. The beam of neutral reactants and products is skimmed into a differentially pumped chamber and ionized by a separated VUV laser beam (118 nm, 10.5 eV per photon). The 118 nm laser light is generated by focusing the third harmonic (355 nm, ~30 mJ) of a Nd³⁺:YAG laser in a tripling cell that contains about a 250 Torr argon–xenon (10/1) gas mixture. An MgF₂ prism (Crystaltechno Ltd, Russia, 6° apex angle) is placed into the laser beam to enhance separation of the generated 118 nm laser beam from the 355 nm input laser beam. After the near threshold ionization, photoions are detected by a TOFMS.

B. Computational procedures

The highly spin-polarized 3d4s electrons of iron give rise to directional bonding, magnetism, and Jahn–Teller distortions, yielding structures for which the bonding is maximized but high magnetic moments still remain, coupled ferromagnetically.⁶⁷ For bi-nuclear species, spin coupling between electrons in d-orbitals of different Fe centers adds further complexity. Wave function based methods like complete active space self consistent field (CASSCF) and multireference configuration interaction (MRCI) require large basis sets, orbital spaces, number of electrons, and extensive treatment of electron correlation (a very large number of configurations) to reach reasonable accuracy.⁵² In this work, calculations of the structural parameters for neutral Fe_mS_n clusters and the hydrogenation reactions of CO on Fe₂S₂ clusters are performed employing density functional theory (DFT). The hybrid B3LYP exchange–correlation functional,⁶⁸⁻⁷⁰ which has also been used in previous studies on Fe compounds,⁷¹⁻⁷³ and the SVP [5s4p2d/4s3p1d] basis set⁷⁴ for Fe–S from the library of optimized basis sets of the Ahlrichs group, which was used in studies of structure and thermochemistry of Fe₂S₂^{-0/+} clusters,⁵² are adopted.

Binding energies between neutral Fe_mS_m and CO are calculated at different typical association geometries to obtain the lowest energy structures of the Fe_mS_mCO clusters. The calculations for the potential energy surfaces (PESs) of the hydrogenation reactions of CO on Fe₂S₂, involve geometry optimizations of the reactants, intermediates, transition states, and products. Vibrational frequency calculations are further performed to confirm the global minima ground states and transition states, which have zero and one imaginary frequencies, respectively. Additionally, intrinsic reaction coordinate (IRC) calculations are carried out to determine that an estimated transition state connects two appropriate local minima along the reaction pathway. Binding energies are calculated for a few species employing the Basic Set Superposition Error (BSSE) correction:^{75,76} these corrections are found to be insignificant at the present level of theory.

Results

A. Experimental results

Fig. 1 presents a typical TOF mass spectrum of neutral iron sulfide Fe_mS_n ($m = 1-6$, $n = 1-6$) clusters generated by laser ablation of a pressed iron-sulfur (mole ratio Fe/S = 4) powder target into a pure He carrier gas, and ionized by 118 nm laser radiation. In Fig. 1, the most intense mass peaks for the iron sulfide series are FeS , Fe_2S_2 , Fe_3S_3 , and Fe_4S_4 . The relatively high Fe_mS_n signal intensities are at $n = m$ for $m = 1-4$: under these conditions, both sulfur poor ($n \leq m$) and rich ($n > m$) clusters can be observed. Some pure sulfur clusters S_m and oxygen containing clusters $\text{Fe}_m\text{S}_n\text{O}_x$ are also observed, because sulfur powder is used as the sulfur source and trace amounts of oxygen impurity may be contained in the pressed powder target and carrier gas. Various other Fe/S ratio targets are also prepared and used in the experiment. The spectra are similar to the one shown in Fig. 1 for Fe/S mole ratios in the range of 1 to 8. At low Fe/S ratios (Fe/S = 1), sulfur rich clusters and pure sulfur clusters S_m become a relatively more intense presence in the mass spectra. At high Fe/S ratios (Fe/S = 8), sulfur poor clusters become relatively intense and pure iron clusters, such as Fe_2 , are observed.

Mass spectra generated from the reaction of neutral iron sulfide clusters with 20% CO seeded in He gas in a fast flow reactor are presented in Fig. 2(b). By way of comparison, Fig. 2(a) shows the TOFMS for Fe_mS_n clusters reacting with only He in the reaction cell. If pure He gas is added to the reactor cell, all cluster signals decrease in roughly the same proportion due to scattering by the inert gas in the reactor (Fig. 2(a)). An association product $\text{Fe}_2\text{S}_2\text{CO}$ is observed when 20% CO/He is added to the fast flow reactor. It is generated from the association reaction, $\text{Fe}_2\text{S}_2 + \text{CO} \rightarrow \text{Fe}_2\text{S}_2\text{CO}$, and is stabilized (cooled) by third body (usually He) collisions. About a 65% decrease in intensity of the FeS cluster mass peak is observed after reaction with CO, but no association product is observed: this observation suggests a possible reaction, $\text{FeS} + \text{CO} \rightarrow \text{Fe} + \text{OCS}$.

The reactions of Fe_mS_n clusters with ^{13}CO and H_2 generate two new clusters: the adduct of ^{13}CO and one H_2 molecule to form the product $\text{Fe}_2\text{S}_2\text{COH}_2$; and the adduct of ^{13}CO and two

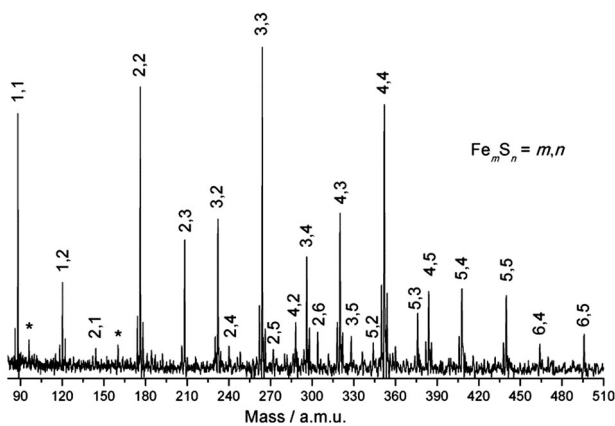


Fig. 1 Neutral iron sulfide Fe_mS_n ($m = 1-6$, $n = 1-6$) distribution detected by 118 nm single photon ionization and time of flight mass spectrometer.

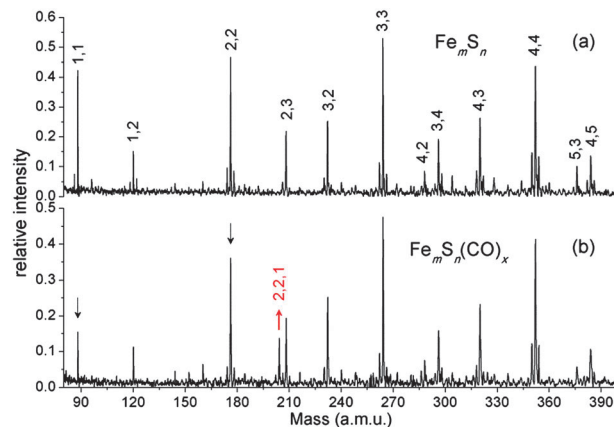
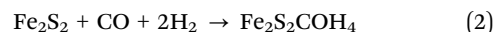
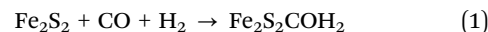


Fig. 2 Neutral iron sulfide cluster distributions after reaction and collision with (a) pure helium, and (b) 20% CO/He, in a fast flow reactor. Products are labeled as $\text{Fe}_m\text{S}_n(\text{CO})_x$ (m, n, x). See text for details.

H_2 molecules to form the product $\text{Fe}_2\text{S}_2\text{COH}_4$ (Fig. 3). The general reactions are



These experimental results suggest that Fe_2S_2 clusters are reactive with the CO- H_2 gas mixture and that the Fe_2S_2 cluster could be a catalyst for the CO hydrogenation reaction. In order to explore and elucidate this interpretation, the reaction

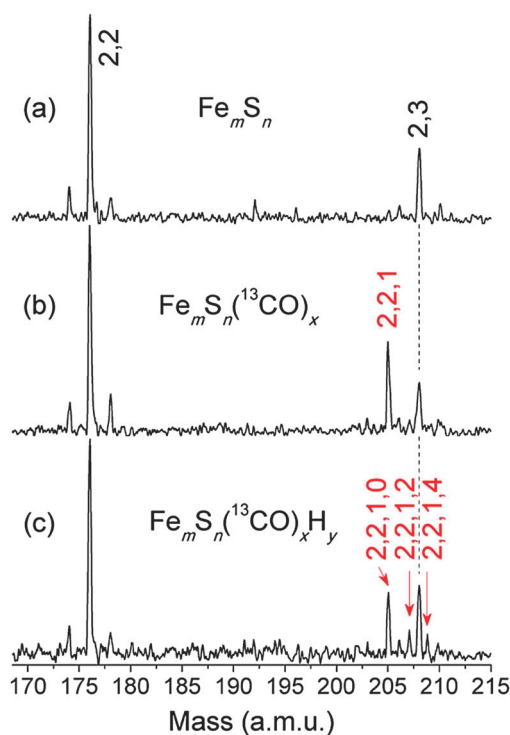


Fig. 3 Product distribution for the reaction of neutral Fe_2S_2 clusters with (a) pure helium, (b) 20% $^{13}\text{CO}/\text{He}$, and (c) 20% $^{13}\text{CO}/\text{H}_2$, in a fast flow reactor. Products are labeled as $\text{Fe}_m\text{S}_n(^{13}\text{CO})_x\text{H}_y$ (m, n, x, y). See text for details.

energies, mechanisms, and potential energy surfaces for the $\text{Fe}_2\text{S}_2 + \text{CO} + \text{H}_2$ reaction system are calculated. Theoretical results can supply more information as discussed in next section.

B. Theoretical results

To investigate reactions of neutral $(\text{FeS})_m$ clusters with CO, binding energies and bond lengths for Fe–C bonds of $(\text{FeS})_m\text{-CO}$ ($m = 1\text{--}4$) clusters are calculated and listed in Table 1: binding energies are defined as $E((\text{FeS})_m) + E(\text{CO}) - E((\text{FeS})_m\text{CO})$. The PESs and the optimized geometries of reaction intermediates and transition states calculated by DFT for the reaction ${}^5\text{FeS} + \text{CO} \rightarrow {}^5\text{Fe} + \text{OCS}$ is presented in Fig. 4. The most stable adsorption structure is for the C atom of CO to be bonded directly to the iron atom in the FeS cluster. A sulfur transfer reaction occurs from the FeS moiety to carbon *via* TS1. The mechanism is barrierless as presented in Fig. 4.

In order to study the mechanism of CO hydrogenation with Fe_mS_n cluster species theoretically, DFT calculations are performed for the reaction $\text{CO} + 2\text{H}_2 \rightarrow \text{CH}_3\text{OH}$ on Fe_2S_2 cluster. Pure H_2 gas in the fast flow reactor is investigated as reference: hydrogen association products are not intense and not as stable as CO association products as shown in Fig. 2(b). This experimental result suggests that Fe_2S_2 clusters are more active with CO than with H_2 . Therefore, in a competitive environment, CO will preferentially adsorb on Fe_2S_2 clusters as the first step, rather than H_2 , in the hydrogenation process.

Table 1 Binding energies of neutral $(\text{FeS})_m\text{-CO}$ ($m = 1\text{--}4$) clusters, and bond lengths of Fe–C bond as calculated by B3LYP/SVP

$(\text{FeS})_m(\text{CO})$	Binding energy (eV)	Fe–C bond length (Å)
$m = 1$	1.14	1.903
$m = 2$	1.16	1.982
$m = 3$	0.62	2.045
$m = 4$	0.74	2.042

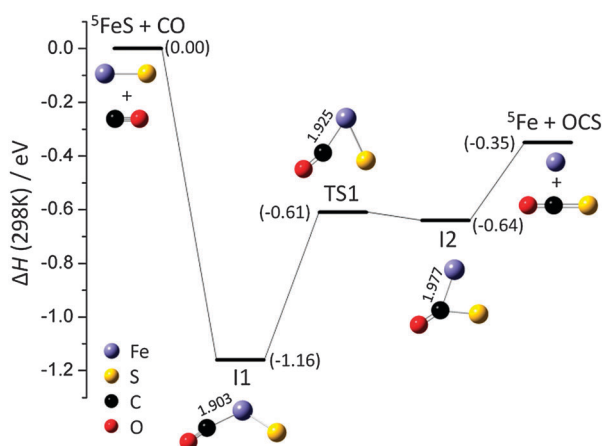


Fig. 4 A potential energy surface profile for the reaction ${}^5\text{FeS} + \text{CO} \rightarrow {}^5\text{Fe} + \text{OCS}$. Energies are in eV and relative to the initial reactant energy of ${}^5\text{FeS} + \text{CO}$. Energy levels are calculated by B3LYP/SVP. The spin multiplicity (M) is listed as ${}^M\text{FeS}$; the Fe–C bond length values in Å are given.

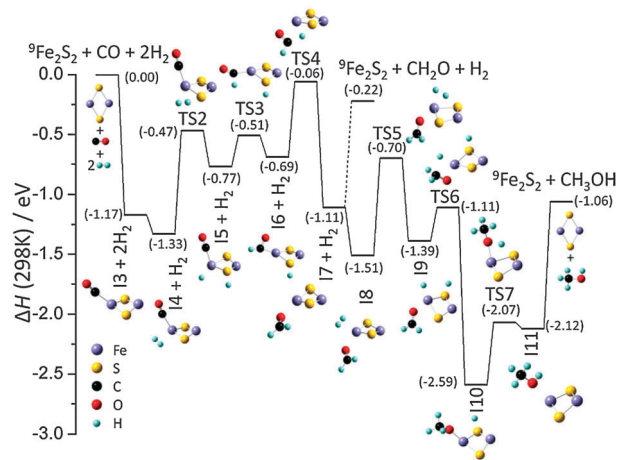


Fig. 5 A potential energy surface profile for the reaction ${}^9\text{Fe}_2\text{S}_2 + \text{CO} + 2\text{H}_2 \rightarrow {}^9\text{Fe}_2\text{S}_2 + \text{CH}_3\text{OH}$. Energies are in eV and relative to the initial reactant energy of ${}^9\text{Fe}_2\text{S}_2 + \text{CO} + 2\text{H}_2$. Energy levels are calculated by B3LYP/SVP. The spin multiplicity (M) is listed as ${}^M\text{Fe}_2\text{S}_2$. The release of formaldehyde from I7 and methanol from I11 require 0.89 eV and 1.06 eV energies, respectively. See text for details.

Fig. 5 presents the reaction pathway for CO hydrogenation on a Fe_2S_2 cluster. CO bonds to the Fe atom of Fe_2S_2 to form intermediate I3, and then the first hydrogen molecule attacks the same Fe atom to form intermediate I4. The H–H bond of hydrogen molecule ruptures, and one hydrogen atom transfers to sulfur *via* transition state TS2 to form I5. Through transition states TS3 and TS4, hydrogen atoms of the –FeH and –SH moieties transfer to CO and yield intermediate I7, for which the O atom of formed formaldehyde bonds to the Fe atom of Fe_2S_2 . At this point in the catalytic synthesis, the release of formaldehyde CH_2O from the Fe_2S_2 cluster requires 0.89 eV: a mixture of CO and H_2 with a 1:1 or less mole ratio could generate a product mixture rich in formaldehyde. The formation of methanol proceeds as a second hydrogen molecule attaches to the Fe atom to which the formed formaldehyde is bonded. The lowest energy adsorption structure is found as intermediate I8. Through transition state TS5, the H–H bond ruptures and yields intermediate I9, which contains –FeH and –SH moieties. The H atom of –FeH moiety transfers to formaldehyde and forms CH_3O bonded to the Fe atom. Then the H atom of –SH moiety transfers to the CH_3O through transition states TS7: intermediate I10 transforms to intermediate I11, in which methanol is attached to Fe_2S_2 by an association energy of ~ 1 eV.

Discussion

A. Reactions of $(\text{FeS})_m$ with CO

Three types of reactions are identified for the interaction of $(\text{FeS})_m$ cluster with CO in the flow tube reactor experiments presented in Fig. 2. First, the reaction of FeS clusters with CO to form carbonyl sulfide is observed. Second, for Fe_2S_2 clusters, the association product $\text{Fe}_2\text{S}_2\text{CO}$ is observed. Third, for Fe_3S_3 and Fe_4S_4 clusters, neither reaction nor association products are detected. This size dependent behavior indicates the diverse

reactivities and properties existing for the interactions of $(\text{FeS})_m$ clusters with CO, as discussed below for these distinct cases.

(1) For $m = 1$, after reaction with CO, the intensity of FeS cluster mass peak decreases by about 65%, but no association product is observed. This experimental result indicates that the barrier for the reaction of FeS clusters with CO must be lower than the initial reactant energy of FeS + CO. In the flow tube reactor, Fe_mS_n clusters generated from laser ablation are cooled to ~ 300 – 400 K due to a large number of collisions with the helium buffer gas. Therefore, if a high barrier were to exist for the further reaction of FeS clusters with CO, association products FeS(CO) should be observed in the mass spectrum (Fig. 2). As the PES profile for the reaction $\text{FeS} + \text{CO} \rightarrow \text{Fe} + \text{OCS}$ calculated and presented in Fig. 4, the transfer of the S atom leads to Fe(OCS) *via* TS1 and finally generates product Fe + OCS. Based on DFT calculations, the overall reaction of $\text{FeS} + \text{CO} \rightarrow \text{Fe} + \text{OCS}$ is barrierless and thermodynamically favorable. Free OCS molecules cannot be detected by single photon ionization from a 118 nm laser—the ionization energy of OCS is ~ 11.2 eV.⁷⁷ The calculated result is consistent with the experimental result.

(2) For $m = 2$, only association products $\text{Fe}_2\text{S}_2\text{CO}$ are observed, indicating that the binding energy between Fe_2S_2 and CO is large enough to stabilize the $\text{Fe}_2\text{S}_2\text{CO}$ association cluster under the cooling collisional conditions in our flow tube reactor experiment. As the calculation result shown in Fig. 4, formation of carbonyl sulfide from reaction of CO with FeS must involve a sulfur atom transfer from iron atom to carbon atom. A relatively long distance between the associated Fe_2S_2 and CO moieties (1.982 Å compared to 1.903 Å for FeS–CO, shown in Table 1) indicates a relatively high barrier for the sulfur atom transfer from iron to carbon. In other hand, the sulfur atom in the Fe_2S_2 cluster form bonds with both iron atoms, so the sulfur transfer will need to break two Fe–S bonds in order to occur. It also makes the sulfur transfer harder than that in FeS + CO reaction. Thus, only association products are observed for $\text{Fe}_2\text{S}_2 + \text{CO}$ in the flow tube experiment.

(3) For $m = 3$ and 4, intensity of $(\text{FeS})_{3,4}$ cluster peaks do not distinctly decrease, and no association products $(\text{FeS})_{3,4}\text{CO}$ are observed in the mass spectrum of $\text{Fe}_m\text{S}_n + \text{CO}$, as shown in Fig. 2(b). This experimental result suggests that the reactivity of $(\text{FeS})_{3,4}$ clusters toward CO is smaller than that of $(\text{FeS})_{1,2}$ clusters. The binding energy of CO with larger clusters $(\text{FeS})_{3,4}$ is also small: the calculated binding energies (~ 0.7 eV) of CO with $(\text{FeS})_{3,4}$ are less than those of $(\text{FeS})_{1,2}$ (~ 1.1 eV, Table 1). The larger clusters may be hotter than the smaller ones due to cluster growth processes and may also be harder to cool in the expansion: thus the reduced binding energy, the cluster temperature, and the reduced cooling of the larger clusters all contribute to the absence of $(\text{FeS})_{3,4}\text{CO}$ cluster in the TOFMS data.

B. Methanol and formaldehyde formation from reaction of CO and H₂ on Fe₂S₂ clusters

Since the position of mass peaks of $\text{Fe}_2\text{S}_2\text{COH}_2$ and $\text{Fe}_2\text{S}_2\text{COH}_4$ are overlapped with those of $^{54}\text{FeFeS}_3$ and Fe_2S_3 , respectively,

^{13}CO is employed to study the CO hydrogenation reactions on Fe_2S_2 clusters. In addition to ^{13}CO association products $\text{Fe}_2\text{S}_2^{13}\text{CO}$ observed for the reaction of $\text{Fe}_2\text{S}_2 + ^{13}\text{CO} + \text{H}_2$, new products, $\text{Fe}_2\text{S}_2^{13}\text{COH}_2$ and $\text{Fe}_2\text{S}_2^{13}\text{COH}_4$ are observed in Fig. 3. Molecular adsorption of CO and 1 or 2 H₂ molecules on the Fe_2S_2 cluster allows formaldehyde and methanol to be formed by the CO hydrogenation reactions that are thermodynamically and dynamically favorable at room temperature in the fast flow reactor (at *ca.* 300–400 K) (see Fig. 5). As the calculation results for the reaction pathways of CO hydrogenation on Fe_2S_2 clusters indicate, CO is adsorbed on Fe atom of Fe_2S_2 clusters in the first step of the reaction. The lowest energy structures of the association products FeS(CO) (shown in Fig. 4) also indicate that the CO binds with FeS clusters through Fe atoms. These results suggest that the Fe atoms of the reactive Fe_mS_n clusters are the active sites for adsorption of CO.

In the experimental results (Fig. 2 and 3), CO association and hydrogenation products are observed on Fe_2S_2 clusters, but are not observed on FeS clusters. From the spin density profiles for $(\text{FeS})_{1,2}(\text{CO})_{0,1}$ and $\text{Fe}_2\text{S}_2\text{COH}_2$ in Fig. 6, electrons are mostly localized on Fe sites: these are the most active sites in the $(\text{FeS})_{1,2}$ clusters. The CO molecule can thus be adsorbed to these active Fe atoms of $(\text{FeS})_{1,2}$ clusters as demonstrated for reaction pathways presented in Fig. 4 and 5. After the active Fe atoms of $(\text{FeS})_{1,2}$ clusters adsorb a CO molecule, the spin density distributions on these Fe atoms change. The distribution of spin density on the Fe atom of the $\text{Fe}_2\text{S}_2\text{CO}$ cluster is increased to 3.832 compared with that of an Fe atom of an Fe_2S_2 cluster (3.646 shown in Fig. 6); an H₂ molecule can therefore adsorb to this more active Fe atom of the $\text{Fe}_2\text{S}_2\text{CO}$ cluster. As the spin density profile of $\text{Fe}_2\text{S}_2(\text{CO})(\text{H}_2)$ shows, the slightly increased distribution of spin density on S atoms (0.367 compared to that of an S atom of Fe_2S_2 (0.354) and $\text{Fe}_2\text{S}_2\text{CO}$ (0.333)) can contribute to the H–H bond rupture process, in which one H atom transfers from iron to sulfur as shown in Fig. 5 from I4 to I5 through TS2.

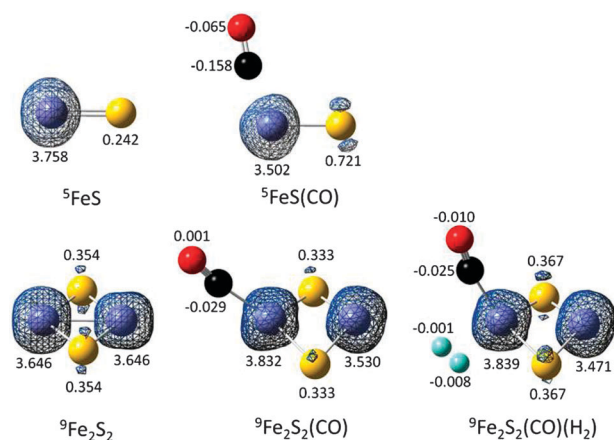


Fig. 6 Spin density profiles for $^M(\text{FeS})_{1,2}$, $^M(\text{FeS})_{1,2}(\text{CO})$ and $^M\text{Fe}_2\text{S}_2(\text{CO})(\text{H}_2)$ clusters. The superscript M indicates the spin multiplicity. Sum of Mulliken atomic spin densities of $^5\text{FeS}(\text{CO})_{0,1}$ and $^9\text{Fe}_2\text{S}_2(\text{CO})_{0,1}(\text{H}_2)_{0,1}$ are 4.000 and 8.000, respectively.

With a CO molecule adsorbed on the active Fe atom of a FeS cluster, the electronic distribution is different than that just described. The spin density distribution on the Fe atom decreases to 3.502 compared to that of the Fe atom in an FeS cluster (3.758), and the distribution of spin density on sulfur in an FeS(CO) cluster (0.721) increases almost three times compared to that of the sulfur atom in an FeS cluster (0.242) (see Fig. 6). The increased spin density of the sulfur atom in an FeS(CO) cluster will enhance its interaction with the carbon atom of the adsorbed CO, which bonds with the Fe atom; consequently, the S atom transfer to the C atom and formation of OCS + Fe is the main reaction path, as displayed in Fig. 4.

After CO molecules adsorb on catalytic Fe₂S₂ clusters, the next step of the hydrogenation reaction is an H₂ molecule adsorbs on the Fe₂S₂CO cluster, as discussed above. The H–H bond of the adsorbed H₂ molecule ruptures: one of the H atom stays at the Fe atom site and forms a –FeH moiety; and the other H atom transfers to an S atom and forms a –SH moiety. These two hydrogen atoms transfer from –FeH and –SH moieties to the CO ligand, one by one, by surmounting a barrier to transition states TS3 and TS4, and thereby forming Fe₂S₂(CH₂O). The formaldehyde thus formed in the catalytic reaction of carbon monoxide and hydrogen, is also found to be the key intermediate to yield surface-bound methanol during condensed phase catalytic reactions.^{78,79} Subsequently, another adsorbed hydrogen molecule is dissociated on the Fe atom of the Fe₂S₂(CH₂O) cluster, as one hydrogen atom transfers to an S atom and the another one remains on the Fe atom. The H atom from the –FeH moiety transfers to the CH₂O ligand, and stable intermediate, Fe₂S₂H(CH₃O) (2.59 eV lower than the initial energy), is formed, as shown in Fig. 5. The transfer of the last H atom leads to Fe₂S₂(CH₃OH) via TS7 and finally generates products Fe₂S₂ + CH₃OH. Based on the DFT calculations, the overall reaction of Fe₂S₂ + CO + 2H₂ → Fe₂S₂ + CH₃OH is barrierless and thermodynamically favorable. Free CH₃OH molecules cannot be detected by single photon ionization from a 118 nm laser—the ionization energy of CH₃OH is ~10.9 eV.^{80,81} Moreover, a hot CH₃OH scattered out of the molecular beam would not readily transit the skimmer and enter the TOFMS chamber for detection by any ionizing photon.

In summary, our calculational and experimental results indicate that Fe atoms of catalytic Fe₂S₂ clusters are the active sites for holding CO and H₂ molecules during the CO hydrogenation reaction process; the H–H bond of the adsorbed H₂ molecule can rupture after absorption on active Fe sites. The hydrogen atoms of either –FeH and –SH moieties can then transfer to CO and CH₂O ligands to yield the important intermediate Fe₂S₂(CH₂O) and Fe₂S₂(CH₃OH) in a stepwise process. The calculated enhanced electron spin density on Fe and S atoms of catalytic Fe₂S₂ clusters apparently contribute to the adsorption of CO and H₂, and dissociation of H–H bonds of adsorbed H₂ molecules.

In the practical catalytic synthesis of methanol through hydrogenation reaction of carbon monoxide, the catalyst must be involved in a cyclic reaction. Fig. 7 presents model catalytic cycles (I and II) employing the Fe₂S₂ site as a catalyst for

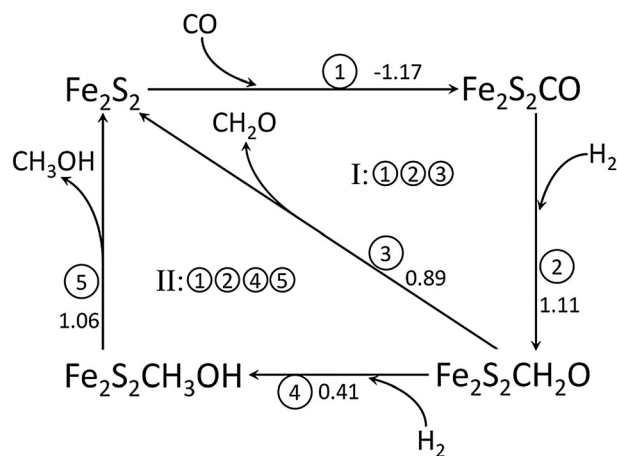


Fig. 7 Catalytic cycles for formaldehyde and methanol formation from reaction of carbon monoxide and hydrogen over neutral Fe₂S₂ clusters in the gas phase. The overall reaction barriers (ΔH_{ORB}) in eV for each elementary step are given (according to Fig. 5).

formaldehyde and methanol syntheses. The reaction pathway is discussed above as given in Fig. 5. The formaldehyde formation process is suggested to be the rate limiting step of both cycles I and II, because, of all the calculated reaction barriers (ΔH_{ORB}) for each elementary step shown in Fig. 7, the formation of the formaldehyde ligand from CO hydrogenation (elementary step 2) is subject to the highest barrier (1.11 eV).

Catalytic clusters in the gas phase can be seen as a good model system for the active site that exists on a catalyst surface. Since Fe₂S₂ clusters are found to have high catalytic activity for hydrogenation reactions of CO to form formaldehyde and methanol at low temperature, iron sulfide can be suggested to be an excellent catalyst for low temperature catalytic syntheses of formaldehyde and methanol. On an iron sulfide catalyst surface, the exposed Fe₂S₂ moieties are proposed to be active sites based on our related gas phase studies. Further research on formaldehyde and methanol syntheses over condensed phase iron sulfide surfaces should be explored.

Conclusions

Reaction of CO with H₂ on neutral Fe_mS_n clusters in the gas phase is explored by employing a flow tube reactor, a time of flight mass spectrometer with 118 nm single photon ionization, and DFT calculations. A strong size dependent reactivity of (FeS)_m clusters toward CO is characterized: an association reaction is observed for the Fe₂S₂ cluster; the reaction FeS + CO → Fe + OCS is found for the FeS cluster; and no association products are observed on (FeS)_{3,4} clusters due in part to their weaker interaction with CO molecules. Products Fe₂S₂¹³COH₂ and Fe₂S₂¹³COH₄ are identified for reactions of ¹³CO with H₂ on Fe_mS_n clusters; this chemistry suggests that Fe₂S₂ clusters have high catalytic activity for hydrogenation reactions of CO to form formaldehyde and methanol. DFT calculations are additionally performed and the following conclusions can be drawn from the theoretical studies: (1) neutral carbonyl sulfide (OCS) is

suggested to be generated from the reactions of FeS with CO at room temperature; (2) reaction of $\text{Fe}_2\text{S}_2 + \text{CO} + 2\text{H}_2 \rightarrow \text{Fe}_2\text{S}_2 + \text{CH}_3\text{OH}$ is barrierless and thermodynamically favorable, and the formaldehyde formed on the reaction potential energy surface is a very important intermediate for the methanol formation; and (3) the Fe atoms are active sites for $(\text{FeS})_{1,2}$ clusters to attach CO molecules. The H_2 molecule is also predicted to be adsorbed on Fe sites of Fe_2S_2 clusters. The attached H_2 molecule dissociates on the active Fe site, and one H atom transfers to the adjacent S site to form $-\text{FeH}$ and $-\text{SH}$ moieties. Electron spin density on Fe and S atoms is correlated with the adsorption of CO and H_2 , and also with dissociation of adsorbed H_2 . The various reaction mechanisms explored by DFT are in good agreement with the experimental results. The exposed Fe_2S_2 units on an iron sulfide catalyst surface are suggested to be active sites for methanol synthesis through reaction of carbon monoxide and hydrogen.

Acknowledgements

This work is supported by a grant from the US Air Force Office of Scientific Research (AFOSR) through grant number FA9550-10-1-0454, the National Science Foundation (NSF) ERC for Extreme Ultraviolet Science and Technology under NSF Award No. 0310717, and the National Science Foundation through XSEDE resources under grant number TG-CHE110083.

Notes and references

- X. M. Liu, G. Q. Lu, Z. F. Yan and J. Beltramini, *Ind. Eng. Chem. Res.*, 2003, **42**, 6518–6530.
- S. Wasmus and A. Kuver, *J. Electroanal. Chem.*, 1999, **461**, 14–31.
- L. Carrette, K. A. Friedrich and U. Stimming, *ChemPhysChem*, 2000, **1**, 162–193.
- M. T. Xu, J. H. Lunsford, D. W. Goodman and A. Bhattacharyya, *Appl. Catal., A*, 1997, **149**, 289–301.
- N. D. Parkyns, C. I. Warburton and J. D. Wilson, *Catal. Today*, 1993, **18**, 385–442.
- F. A. P. Cavalcanti, A. Y. Stakheev and W. M. H. Sachtler, *J. Catal.*, 1992, **134**, 226–241.
- J. R. Wilson and G. Burgh, *Energizing our future: Rational choices for the 21st century*, Wiley, 2007.
- G. A. Olah, A. Goepfert and G. K. S. Prakash, *Beyond oil and gas: The methanol economy*, Wiley-VCH, 2006.
- N. Tsubaki, M. Ito and K. Fujimoto, *J. Catal.*, 2001, **197**, 224–227.
- M. Marchionna, M. Lami and A. M. P. Galletti, *CHEMTECH*, 1977, **27**, 27–31.
- W. J. Shen, Y. Ichihashi and Y. Matsumura, *Appl. Catal., A*, 2005, **282**, 221–226.
- W. J. Shen, Y. Ichihashi and Y. Matsumura, *Catal. Lett.*, 2002, **83**, 33–35.
- W. J. Shen, Y. Ichihashi, M. Okumura and Y. Matsumura, *Catal. Lett.*, 2000, **64**, 23–25.
- S. Marengo, R. Psaro, C. Dossi, S. Calmotti and R. DellaPergola, *Promotion effects in methanol synthesis over MgO-supported Fe-Ir catalysts prepared from mixed-metal clusters*, 1996.
- S. Fujita, M. Usui, H. Ito and N. Takezawa, *J. Catal.*, 1995, **157**, 403–413.
- M. E. Fakley, J. R. Jennings and M. S. Spencer, *J. Catal.*, 1989, **118**, 483–486.
- V. E. Ostrovskii, A. A. Dyatlov and T. P. Ogneva, *Kinet. Catal.*, 1978, **19**, 410–413.
- A. P. V. Soares and M. F. Portela, *Catal. Rev. Sci. Eng.*, 2005, **47**, 125–174.
- M. P. House, A. F. Carley and M. Bowker, *J. Catal.*, 2007, **252**, 88–96.
- C. T. Wang and R. J. Willey, *J. Catal.*, 2001, **202**, 211–219.
- M. Bowker, R. Holroyd, A. Elliott, P. Morrall, A. Alouche, C. Entwistle and A. Toerncrona, *Catal. Lett.*, 2002, **83**, 165–176.
- L. J. Gregoriades, J. Dobler and J. Sauer, *J. Phys. Chem. C*, 2010, **114**, 2967–2979.
- M. G. O'Brien, A. M. Beale, S. D. M. Jacques, T. Buslaps, V. Honkimaki and B. M. Weckhuysen, *J. Phys. Chem. C*, 2009, **113**, 4890–4897.
- E. Soderhjelm, M. P. House, N. Cruise, J. Holmberg, M. Bowker, J. O. Bovin and A. Andersson, *Top. Catal.*, 2008, **50**, 145–155.
- S. Yin and E. R. Bernstein, *Int. J. Mass Spectrom.*, 2012, **321**, 49–65.
- M. Schlangen and H. Schwarz, *Catal. Lett.*, 2012, **142**, 1265–1278.
- N. Dietl, M. Schlangen and H. Schwarz, *Angew. Chem., Int. Ed.*, 2012, **51**, 5544–5555.
- X. N. Li, X. N. Wu, X. L. Ding, B. Xu and S. G. He, *Chem.–Eur. J.*, 2012, **18**, 10998–11006.
- M. Y. Jia, B. Xu, X. L. Ding, S. G. He and M. F. Ge, *J. Phys. Chem. C*, 2012, **116**, 24184–24192.
- H. P. Wang, Y. J. Ko, L. G. Garcia, P. Sen, M. R. Beltran and K. H. Bowen, *Phys. Chem. Chem. Phys.*, 2011, **13**, 7685–7691.
- Y. Xie, F. Dong, S. Heinbuch, J. J. Rocca and E. R. Bernstein, *Phys. Chem. Chem. Phys.*, 2010, **12**, 947–959.
- M.-Y. Jia, B. Xu, X.-L. Ding, Y.-X. Zhao, S.-G. He and M.-F. Ge, *J. Phys. Chem. C*, 2012, **116**, 9043–9048.
- M. Komarneni, J. Shan, A. Chakradhar, E. Kadossov, S. Cabrini and U. Burghaus, *J. Phys. Chem. C*, 2012, **116**, 5792–5801.
- L. Holmgren, M. Andersson and A. Rosen, *Surf. Sci.*, 1995, **331**, 231–236.
- M. D. Morse, M. E. Geusic, J. R. Heath and R. E. Smalley, *J. Chem. Phys.*, 1985, **83**, 2293–2304.
- D. M. Cox, K. C. Reichmann, D. J. Trevor and A. Kaldor, *J. Chem. Phys.*, 1988, **88**, 111–119.
- M. R. Zakin, R. O. Brickman, D. M. Cox and A. Kaldor, *J. Chem. Phys.*, 1988, **88**, 3555–3560.
- A. Berces, P. A. Hackett, L. Lian, S. A. Mitchell and D. M. Rayner, *J. Chem. Phys.*, 1998, **108**, 5476–5490.
- Y. Xie, S. G. He, F. Dong and E. R. Bernstein, *J. Chem. Phys.*, 2008, **128**, 044306.

- 40 P. Liu, Y. Choi, Y. X. Yang and M. G. White, *J. Phys. Chem. A*, 2010, **114**, 3888–3895.
- 41 Y. Y. Chen, X. H. Zhao, X. D. Wen, X. R. Shi, M. Dong, J. G. Wang and H. J. Jiao, *J. Mol. Catal. A: Chem.*, 2010, **329**, 77–85.
- 42 H. Beinert, R. H. Holm and E. Munck, *Science*, 1997, **277**, 653–659.
- 43 R. Cammack, *Advances in Inorganic Chemistry*, Academic Press, New York, 1992.
- 44 M. S. Nurmagambetova, M. I. Baikenov, M. G. Meiramov, A. A. Mukhtar, A. T. Ordabaeva and V. A. Khrupov, *Pet. Chem.*, 2001, **41**, 26–29.
- 45 E. Munck and E. L. Bominaar, *Science*, 2008, **321**, 1452–1453.
- 46 D. C. Rees and J. B. Howard, *Science*, 2003, **300**, 929–931.
- 47 R. D. Bryant, F. V. Kloeke and E. J. Laishley, *Appl. Environ. Microbiol.*, 1993, **59**, 491–495.
- 48 K. Koszinowski, D. Schröder and H. Schwarz, *Eur. J. Inorg. Chem.*, 2004, 44–50.
- 49 H. J. Zhai, B. Kiran and L. S. Wang, *J. Phys. Chem. A*, 2003, **107**, 2821–2828.
- 50 K. Koszinowski, D. Schröder, H. Schwarz, R. Liyanage and P. B. Armentrout, *J. Chem. Phys.*, 2002, **117**, 10039–10056.
- 51 O. Hubner and J. Sauer, *J. Chem. Phys.*, 2002, **116**, 617–628.
- 52 O. Hubner and J. Sauer, *Phys. Chem. Chem. Phys.*, 2002, **4**, 5234–5243.
- 53 A. Nakajima, T. Hayase, F. Hayakawa and K. Kaya, *Chem. Phys. Lett.*, 1997, **280**, 381–389.
- 54 N. Zhang, T. Hayase, H. Kawamata, K. Nakao, A. Nakajima and K. Kaya, *J. Chem. Phys.*, 1996, **104**, 3413–3419.
- 55 M. G. G. Fuchs, S. Dechert, S. Demeshko, U. Ryde and F. Meyer, *Inorg. Chem.*, 2010, **49**, 5853–5858.
- 56 Y. J. Fu, X. Yang, X. B. Wang and L. S. Wang, *J. Phys. Chem. A*, 2005, **109**, 1815–1820.
- 57 Y. J. Fu, J. Laskin and L. S. Wang, *Int. J. Mass Spectrom.*, 2007, **263**, 260–266.
- 58 Y. J. Fu, J. Laskin and L. S. Wang, *Int. J. Mass Spectrom.*, 2006, **255**, 102–110.
- 59 X. Yang, S. Q. Niu, T. Ichiye and L. S. Wang, *J. Am. Chem. Soc.*, 2004, **126**, 15790–15794.
- 60 S. Yin, Y. Xie and E. R. Bernstein, *J. Chem. Phys.*, 2012, **137**, 124304.
- 61 S. Yin, Y. Xie and E. R. Bernstein, *J. Phys. Chem. A*, 2011, **115**, 10266–10275.
- 62 S. G. He, Y. Xie, F. Dong, S. Heinbuch, E. Jakubikova, J. J. Rocca and E. R. Bernstein, *J. Phys. Chem. A*, 2008, **112**, 11067–11077.
- 63 S. G. He, Y. Xie, Y. Q. Guo and E. R. Bernstein, *J. Chem. Phys.*, 2007, **126**, 194315.
- 64 F. Dong, S. Heinbuch, Y. Xie, J. J. Rocca and E. R. Bernstein, *Phys. Chem. Chem. Phys.*, 2010, **12**, 2569–2581.
- 65 W. Xue, Z. C. Wang, S. G. He, Y. Xie and E. R. Bernstein, *J. Am. Chem. Soc.*, 2008, **130**, 15879–15888.
- 66 M. E. Geusic, M. D. Morse, S. C. O'Brien and R. E. Smalley, *Rev. Sci. Instrum.*, 1985, **56**, 2123–2130.
- 67 M. Castro, C. Jamorski and D. R. Salahub, *Chem. Phys. Lett.*, 1997, **271**, 133–142.
- 68 A. D. Becke, *Phys. Rev. A*, 1988, **38**, 3098–3100.
- 69 A. D. Becke, *J. Chem. Phys.*, 1993, **98**, 5648–5652.
- 70 C. T. Lee, W. T. Yang and R. G. Parr, *Phys. Rev. B: Condens. Matter Mater. Phys.*, 1988, **37**, 785–789.
- 71 O. Hubner, V. Termath, A. Berning and J. Sauer, *Chem. Phys. Lett.*, 1998, **294**, 37–44.
- 72 M. N. Glukhovtsev, R. D. Bach and C. J. Nagel, *J. Phys. Chem. A*, 1997, **101**, 316–323.
- 73 B. D. Dunietz, M. D. Beachy, Y. X. Cao, D. A. Whittington, S. J. Lippard and R. A. Friesner, *J. Am. Chem. Soc.*, 2000, **122**, 2828–2839.
- 74 A. Schafer, H. Horn and R. Ahlrichs, *J. Chem. Phys.*, 1992, **97**, 2571–2577.
- 75 A. K. Rappe and E. R. Bernstein, *J. Phys. Chem. A*, 2000, **104**, 6117–6128.
- 76 S. F. Boys and F. Bernardi, *Mol. Phys.*, 2002, **100**, 65–73.
- 77 L. S. Wang, J. E. Reutt, Y. T. Lee and D. A. Shirley, *J. Electron Spectrosc. Relat. Phenom.*, 1988, **47**, 167–186.
- 78 J. Weigel, C. Frohlich, A. Baiker and A. Wokaun, *Appl. Catal., A*, 1996, **140**, 29–45.
- 79 E. E. Ortelli, J. M. Weigel and A. Wokaun, *Catal. Lett.*, 1998, **54**, 41–48.
- 80 V. E. Sahini, V. Constantin and I. Serban, *Rev. Roum. Chim.*, 1978, **23**, 479–482.
- 81 W. Tao, R. B. Klemm, F. L. Nesbitt and L. J. Stief, *J. Phys. Chem.*, 1992, **96**, 104–107.